Separation Science and Technology
Publication details, including instructions for authors and subscription information:
http://www.informaworld.com/smpp/title~content=t713708471

Lysine Adsorption on Cation Exchange Resin. II. Column Adsorption/Desorption Behavior and Modeling

Hidetada Nagai[ab]; Giorgio Carta[a]
[a] Department of Chemical Engineering, University of Virginia, Charlottesville, Virginia, USA [b] Technology and Engineering Laboratory, Ajinomoto, Co., Inc., Kawasaki-ku, Kawasaki-shi, Japan

Online publication date: 08 July 2010

To cite this Article Nagai, Hidetada and Carta, Giorgio(2004) 'Lysine Adsorption on Cation Exchange Resin. II. Column Adsorption/Desorption Behavior and Modeling', Separation Science and Technology, 39: 16, 3711 — 3738
To link to this Article: DOI: 10.1081/SS-200041093
URL: http://dx.doi.org/10.1081/SS-200041093

SEPARATION SCIENCE AND TECHNOLOGY
Vol. 39, No. 16, pp. 3711–3738, 2004

Lysine Adsorption on Cation Exchange Resin. II. Column Adsorption/Desorption Behavior and Modeling

Hidetada Nagai[1,2] and Giorgio Carta[1,*]

[1]Department of Chemical Engineering, University of Virginia, Charlottesville, Virginia, USA
[2]Ajinomoto, Co., Inc., Technology and Engineering Laboratory, Kawasaki-ku, Kawasaki-shi, Japan

ABSTRACT

Column adsorption and desorption of lysine on the strong acid cation exchanger Dowex HCR-W2 are studied experimentally and theoretically. The lysine breakthrough curves have a complex behavior that depends on the pH of the feed solution. At high pH, when lysine is predominately monovalent, an equilibrium binding capacity approaching the total resin ion exchange capacity is obtained but the breakthrough curve is gradual. Conversely, at low feed pH, when lysine is predominately divalent, a sharper breakthrough curve is obtained but the equilibrium binding capacity is only about one half of the total resin ion exchange capacity. Finally, at intermediate feed pH, when divalent and monovalent lysine

*Correspondence: Giorgio Carta, Department of Chemical Engineering, University of Virginia, Charlottesville, VA, USA; E-mail: gc@virginia.edu.

DOI: 10.1081/SS-200041093 0149-6395 (Print); 1520-5754 (Online)

forms coexist in the feed solution, a breakthrough curve comprising an initial gradual wave followed by a plateau and then by a sharper front is obtained. A local equilibrium model is developed to describe the wave shapes. The model is in agreement with the experimentally observed wave shapes although it only affords a qualitative prediction of the effluent concentration profiles. A rate model, taking into account the coupled diffusion of lysine cations, ammonium ion, potassium ion, and hydrogen ion in the resin as well as the reversible interconversion of divalent and monovalent lysine, is thus developed for a quantitative prediction. The rate model is in excellent agreement with experimental effluent concentration profiles and provides a means to rationally design and optimize lysine ion exchange processes.

Key Words: Column adsorption; Column desorption; Lysine; Breakthrough curves; Equilibrium model; Rate model; Ion exchange processes.

INTRODUCTION

In Part I of this work,[1] we examined the equilibrium and kinetics of lysine ion exchange on a strong acid, styrene-divinylbenzene cation exchanger. Adsorption of lysine was shown to occur via the stoichiometric exchange of divalent lysine cations, monovalent lysine cations, or a combination of both, depending on the composition of the solution. The lysine adsorption isotherm, thus, has a complex shape. Constant co-ion concentration isotherms are favorable at low pH but become S-shaped when the lysine concentration is increased. The mass transfer kinetics, which control the rate of ion exchange, are also complicated by the reversible interconversion of divalent and monovalent lysine species in solution and within the resin phase. Moreover, divalent and monovalent lysine diffuse at very different rates and their fluxes are coupled electrostatically to those of other inorganic counterions.

Industrial application of ion exchange for the recovery and separation of amino acids is ordinarily carried out in fixed beds using either single column[2] or multicolumn simulated moving bed systems.[3] Using a cation exchanger, amino acids, such as lysine, can be loaded at a low pH, where they are favorably adsorbed, and desorbed with an alkaline solution that raises the pH to a value where the amino acid becomes negatively charged. For these conditions, desorption is completely mass transfer controlled, since the negatively charged form is largely excluded from the resin by the Donnan potential effect.

In order to design these processes rationally it is desirable to understand column dynamics and develop accurate models to the effluent profiles as a function of flow rate and feed composition. Both ion exchange equilibria

and mass transfer[4,5] affect column dynamics. Ion exchange equilibrium determines the wave characteristics and is especially critical in the adsorption step. Mass transfer, on the other hand, determines band broadening and is especially important at high flow rates, when the residence time is too short to attain local equilibrium, and in the desorption step, when equilibrium no longer plays a role.

The dynamics of fixed-bed separations of amino acids by ion exchange were examined previously by several authors. Equilibrium stage models were used to simulate displacement chromatography separation of mixtures of neutral and acidic amino acids on cation exchange resins.[6,7] In this approach, the bed is modeled as a series of equilibrium stages and physical dispersion effects are simulated by the associated numerical dispersion. Kawakita et al.[2] used this approach to model lysine ion exchange in cation exchange columns. While computationally straightforward, these models cannot predict mass transfer effects quantitatively and are inadequate for the desorption step, which is typically completely mass transfer controlled.

Local equilibrium models have also been used to describe the displacement separation of amino acid mixtures. An advantage of these models is that the limiting solution attainable in the absence of physical dispersion effects can be obtained directly. Carta and Dinerman,[9] used a local equilibrium model to determine the effects of selectivity reversal on the displacement separation of isoleucine and α-aminobutyric acid. Finally, models taking mass transfer into account explicitly also have been developed for neutral amino acids in cation exchange columns. Saunders et al.[7] and Carta et al.,[10] for example, used detailed intraparticle diffusion models to describe the breakthrough and desorption behavior of phenylalanine and tyrosine on a macroreticular strong acid cation exchanger. While accurate, these models tend to require excessive computation times for practical calculations, making simpler approaches desirable. Melis et al.,[11] for example, developed a lumped model to describe mass transfer effects in the cyclic adsorption–desorption of proline based on a simplified form of the Nernst-Planck model cast in terms of a linear driving force approximation. A related approach, which is more rigorous while retaining an equivalent computational simplicity, was developed by Carta and Lewus[12] based on a film model approximation. In this case, the mass transfer resistance is represented by steady diffusion through a solid film of thickness equal to one fifth of the particle size. Analytical integration of the pertinent diffusion equations along the film thickness provides closed-form rate equations that correctly describe the electrostatic coupling effects of the Nernst-Planck model.

This paper has two main objectives. The first is to develop a local equilibrium model to describe the adsorptive behavior of lysine in a cation exchange resin bed as a function of solution composition. In particular, we are interested

in understanding the influence of the complex isotherm shape on column dynamics. The second objective is to develop a mass transfer model to describe the adsorption-desorption behavior of lysine over a broad range of conditions. While models of this type have been developed for neutral amino acids, the interplay of divalent and monovalent lysine forms poses additional challenges. For this purpose, a model based on the film model approximation of Carta and Lewus[12] is developed in conjunction with equilibrium models and diffusivity data obtained in Part I of this work. In Part III, we will explore the application of this model to simulate the dynamic behavior of multicolumn, simulated moving bed systems for lysine recovery and separation.

MATERIALS AND METHODS

The resin used in this work is Dowex HCR-W2 (Dow Chemical Co., Midland, MI), a typical gel-type poly(styrene-divinylbenzene) cation exchanger with a nominal divinylbenzene (DVB) content of 8% and sulfonic acid functional groups. The mean particle diameter of the hydrogen form resin is 714 μm, the dry-weight is 0.48 g dry/g of hydrated resin, the bead density is 0.65 g dry/cm^3 of hydrated particle, and the total ion exchange capacity is 5.3 ± 0.2 mequiv/g dry H-form resin.[1] L-lysine and other chemicals were obtained as described in Part I of this work.

Column experiments were conducted with glass chromatography columns 1.5 cm in diameter and 10 or 20 cm in length (Spectrum Chromatography, Houston, TX). The columns were packed by slurrying the resin with an equal volume of water and quickly pouring the slurry in followed by flow packing. The packed bed density of these columns was 0.38 ± 0.02 g dry resin/cm^3, determined by emptying a packed column and weighing the oven-dried resin; and the void fraction was 0.41 ± 0.01, based on pulse injections of blue dextran (MW ~2,000,000) detected at 280 nm with a Waters ultraviolet (UV) chromatographic detector. Pulse injections of $NaNO_2$ (also detected with the UV detector but at 254 nm) in either 1 M ammonium hydroxide or ammonium chloride yielded very similar values of the void fraction between 0.40 and 0.42.

Feed solutions containing 0.20 M lysine with chloride concentrations of 0.20, 0.36, or 0.56 M as well as lysine solutions containing small amounts of potassium ion were used in breakthrough experiments while 1 M ammonium hydroxide was used as the desorbent. The feed solutions were prepared from stock solutions of lysine hydrochloride, HCl, and potassium chloride. Syringe-type FPLC pumps (Model P-500, Amersham Biosciences, Uppsala, Sweden) were used to supply the feed and desorbent solutions. The effluent pH was monitored with an online pH meter (LKB, Model

2195-100) while the composition was determined by collecting samples with a Gilson Model 201 fraction collector for high-pressure liquid chromatography (HPLC) analysis as described in Ref.[1].

MODELING AND EXPERIMENTAL RESULTS

Lysine Breakthrough—Local Equilibrium Model

In the following section we consider the breakthrough behavior of lysine, initially in ammonium form, in a cation exchange resin column. As shown in Part I of this work, lysine adsorption involves the exchange of divalent lysine, monovalent lysine, or a combination of both, depending on the solution pH. Ion exchange of the divalent form is favorable but the lysine uptake capacity is limited to about one half of the ion exchange capacity. Conversely, ion exchange of the monovalent form is unfavorable, but the lysine uptake capacity can approach the total ion exchange capacity of the resin.

Assuming plug flow and neglecting axial dispersion, the following bed conservation equations can be written:

$$\rho_b \frac{\partial q_L}{\partial t} + \varepsilon \frac{\partial C_L}{\partial t} + u \frac{\partial C_L}{\partial z} = 0 \tag{1}$$

$$\rho_b \frac{\partial q_N}{\partial t} + \varepsilon \frac{\partial C_N}{\partial t} + u \frac{\partial C_N}{\partial z} = 0 \tag{2}$$

$$z = 0, C_L = C_L^F, C_N = C_N^F \tag{3}$$

$$t = 0, C_L = C_L^0, C_N = C_N^0 \tag{4}$$

where C_L and q_L are the total lysine concentrations in the solution and resin phase, respectively, and C_N and q_N are the corresponding total ammonia concentrations. An additional conservation equation can also be written for the co-ion (chloride in our case). However, assuming that co-ion exclusion from the resin is complete, this equation is trivial.

Equations 1 and 2 are coupled with the solution and ion exchange equilibrium relationships developed in Part I of this work.[1] It should be noted that writing the conservation equations in terms of total lysine and total ammonia is sufficient. In fact, given C_L, C_N, and the co-ion concentration, the electroneutrality condition for the solution phase can be solved providing the pH, and, hence, the speciation of charged lysine and ammonia forms in the solution surrounding the resin particles. In turn this can be used to calculate the resin equilibrium composition via the mass action law relationships governing the ion exchange reactions.[1]

The local equilibrium solution is constructed by mapping characteristics on the hodograph plane C_N, C_L, and then determining the concentration profiles along characteristics using the corresponding characteristic velocities.[4] The latter are obtained as follows. For simple waves we have

$$v_{C_L} = \frac{v}{1 + \rho_b/\varepsilon[(\partial q_L/\partial C_L) + (\partial q_L/\partial C_N)(dC_N/dC_L)]} \tag{5}$$

$$v_{C_N} = \frac{v}{1 + \rho_b/\varepsilon[(\partial q_N/\partial C_L)(dC_L/dC_N) + (\partial q_N/\partial C_N)]} \tag{6}$$

while for shock waves we have

$$v_{s_L} = \frac{v}{1 + \rho_b/\varepsilon[(q'_L - q''_L)/(C'_L - C''_L)]} \tag{7}$$

$$v_{s_N} = \frac{v}{1 + \rho_b/\varepsilon[(q'_N - q''_N)/(C'_N - C''_N)]} \tag{8}$$

The partial derivatives and the q-values appearing in these expressions are evaluated numerically from the ion exchange and solution equilibrium relationships developed in Part I[1] while $'$ and $''$ denote conditions upstream and downstream of the wave.

Coherent paths on the hodograph plane are found by equating the characteristic velocities and determining the slopes dC_N/dC_L.[4,13] For simple waves we obtain

$$\lambda_{\pm} = \left(\frac{dC_N}{dC_L}\right)_{\pm} = \frac{-(\partial q_L/\partial C_L - \partial q_N/\partial C_N) \pm \sqrt{\begin{array}{r}(\partial q_L/\partial C_L - \partial q_N/\partial C_N)^2 \\ +4(\partial q_N/\partial C_L)(\partial q_L/\partial C_N)\end{array}}}{2(\partial q_L/\partial C_N)} \tag{9}$$

where the appropriate value of λ is selected by requiring that the characteristic velocity increases move downstream in the column. Similarly, coherent shock paths are found by equating shock velocities, yielding

$$\frac{q'_L - q''_L}{C'_L - C''_L} = \frac{q'_N - q''_N}{C'_N - C''_N} \tag{10}$$

Starting with known values of upstream concentrations, the downstream concentrations for a coherent shock wave can be found by trial and error from this equation. As for simple waves, only one of the two possible trajectories obtained with this procedure will be physically realistic.

Numerical calculations based on these equations are shown later and compared with experimental lysine breakthrough curves obtained with the same feed lysine concentrations but with different chloride concentrations and, hence, different feed pH. The parameters used are summarized in Table 1 and the three cases considered are shown in Figs. 1–3. In Case 1 (Fig. 1) the lysine feed pH is 5.57, which, as shown in Part I of this paper, corresponds to a predominance of monovalent lysine. In Case 2 (Fig. 2) the lysine feed pH is 0.80, which corresponds to a predominance of divalent lysine. Finally, in Case 3 (Fig. 3) the lysine feed pH is 1.85, which corresponds to a mixture of monovalent and divalent lysine. The following dimensionless variables are defined: $v_c^* = v_c/v$, $v_s^* = v_s/v$, and $RV = \varepsilon/v^*$. The quantity relative volumes (RV) represents the number of column volumes passed. The corresponding hodograph planes are also shown in Figs. 1–3. Point A is the feed and point C is the state downstream of the lysine wave. As the chloride ion is not adsorbed, it moves quickly through the column. Hence, the effluent reaches point C with $C_L = 0$ and $C = C^F_{Cl^-} = 0$ when $RV = \varepsilon$. Of course, the initial conditions prevail for $RV < \varepsilon$.

Table 1. Summary of model parameters.

Parameter	Value	Units
q_0	5.3	mequiv/g
r_p	357	μm
ε	0.41	
ρ_b	0.38	g/cm^3
S_{Lys^{++}/H^+}	5.0	g/cm^3
S_{Lys^+/H^+}	0.75	
$S_{NH_4^+/H^+}$	1.5	
S_{K^+/H^+}	1.9	
pK_1	2.18	M
pK_2	8.95	M
pK_3	10.5	M
pK_N	9.25	M
pK'_1	3.00	M
pK'_N	9.59	M
$D_{Lys^{++}}$	5.0×10^{-8}	cm^2/s
D_{Lys^+}	2.0×10^{-7}	cm^2/s
$D_{NH_4^+}$	1.8×10^{-6}	cm^2/s
D_{K^+}	1.6×10^{-6}	cm^2/s
D_{H^+}	1.0×10^{-5}	cm^2/s
D_{NH_3}	1.9×10^{-6}	cm^2/s

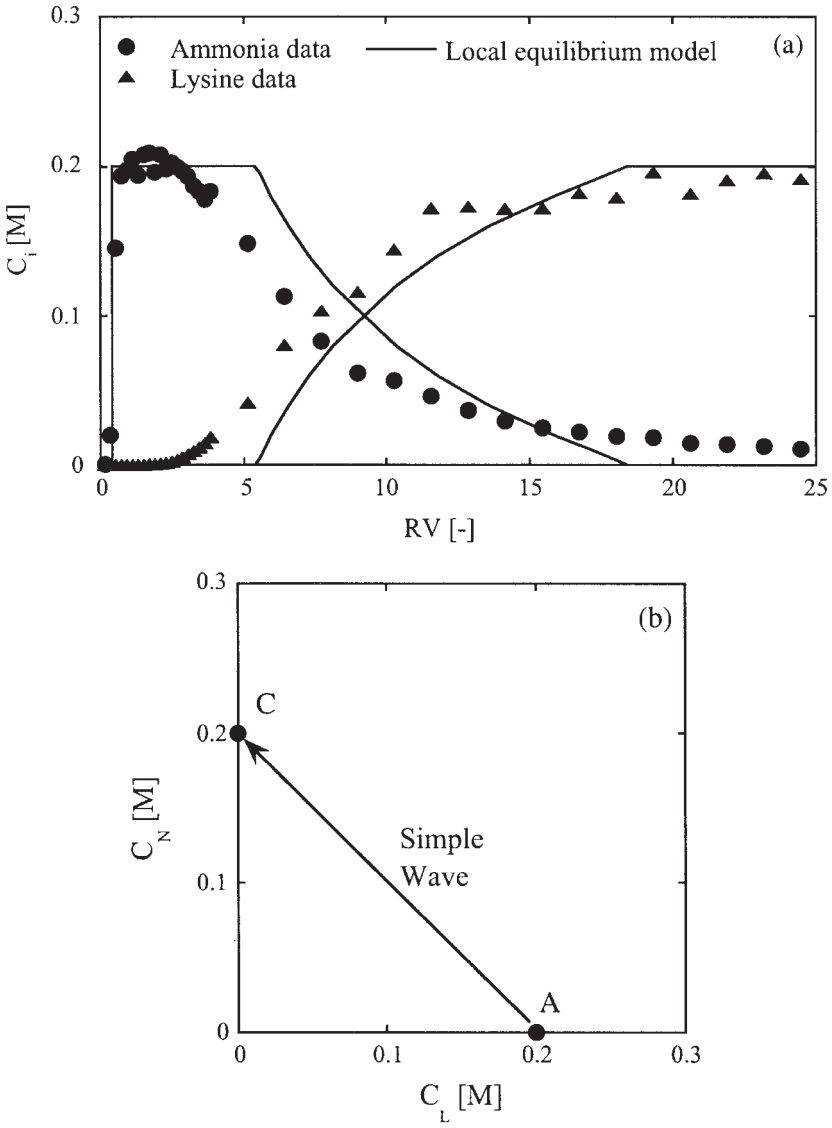

Figure 1. Breakthrough curves for Case 1: $C_L = 0.20\,\text{M}$, $C_{Cl^-} = 0.20\,\text{M}$, pH = 5.57, $u = 0.0072\,\text{cm/s}$, $L = 10\,\text{cm}$. (a) Experimental and predicted effluent profiles, (b) hodograph plane. Lines are calculated from local equilibrium model.

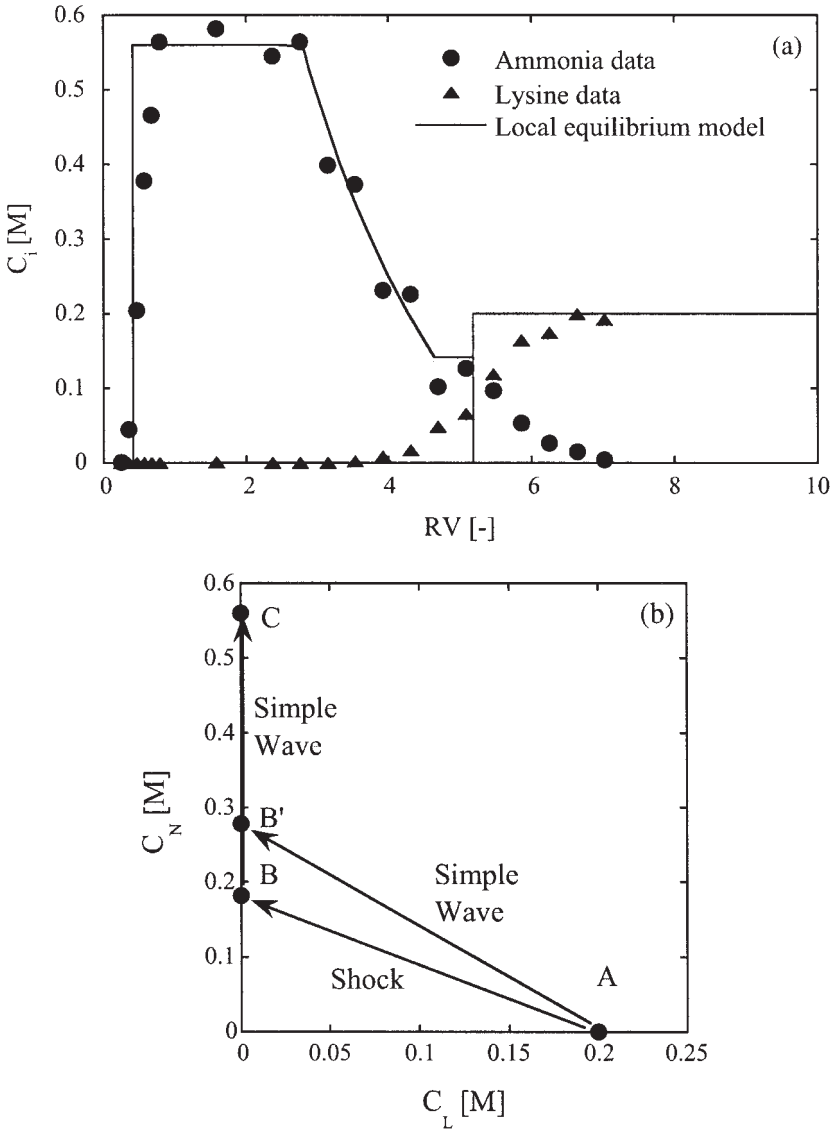

Figure 2. Breakthrough curves for Case 2: $C_L = 0.20\,\mathrm{M}$, $C_{Cl^-} = 0.56\,\mathrm{M}$, pH = 0.80, $u = 0.0072\,\mathrm{cm/s}$, $L = 10\,\mathrm{cm}$. (a) Experimental and predicted effluent profiles, (b) hodograph plane. Lines are calculated from local equilibrium model.

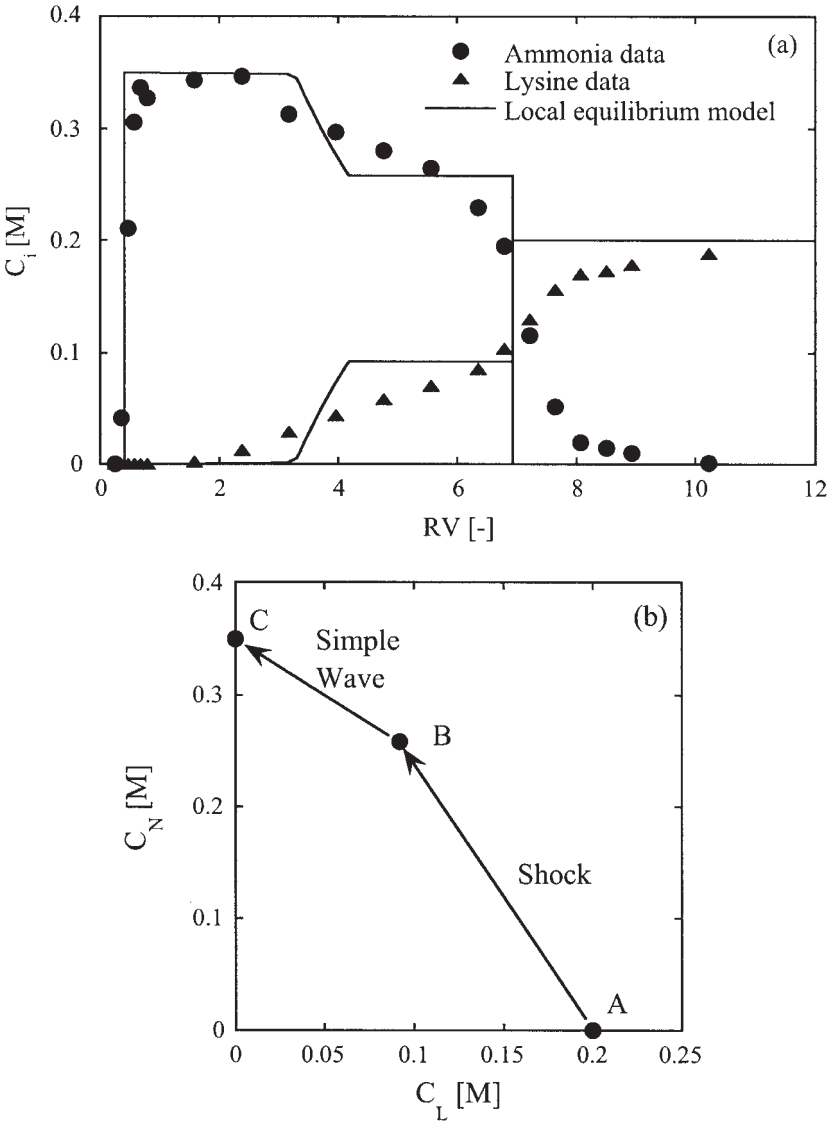

Figure 3. Breakthrough curves for Case 3: $C_L = 0.20\,\text{M}$, $C_{Cl^-} = 0.35\,\text{M}$, pH = 1.85, $u = 0.0072\,\text{cm/s}$, $L = 10\,\text{cm}$. (a) Experimental and predicted effluent profiles, (b) hodograph plane. Lines are calculated from local equilibrium model.

Solution for Case 1

The following values are calculated from Eqs. 9 and 5:

Point	Composition [M]	λ	v^*
A	$C_L = 0.20$, $C_N = 0$	-1.0	0.054
C	$C_L = 0$, $C_N = 0.20$	-1.0	0.19

Since $v_c^*(C) > v_c^*(A)$, a simple wave connects these two states. The concentration profile is calculated by computing the characteristic velocity at each point along the AC path and is shown in Fig. 1a in comparison with experimental results. The gradual nature of the simple wave is evident as even in the absence of mass transfer resistance a smooth profile is observed. This trend is also clearly seen for the experimental curves with the main difference being that the experimental profiles are somewhat more spread out.

Solution for Case 2

The hodograph plane is shown in Fig. 2b. Point A is the feed and the corresponding equilibrium resin composition is $q_L = 2.52\,\text{mmol/g}$ and $q_N = 0\,\text{mmol/g}$. Line AB′ corresponds to a coherent simple wave originating from point A. The following values are calculated from Eqs. 9 and 5:

Point	Composition [M]	λ	v_c^*
A	$C_L = 0.2$, $C_N = 0$	-1.39	0.75
B′	$C_L = 0$, $C_N = 0.279$	∞	0.26

Since $v^*(B') < v_c^*(A)$ a shock is formed between states A and B. The composition of state B is found from Eq. 10 by setting $(q_L/C_L)_A = 2.52/0.20 = (q_N/C_N)_B$, which gives $C_N = 0.14\,\text{M}$, $q_N = 1.79\,\text{mmol/g}$, and $v_{sh}^* = 0.19$. The RV-value corresponding to the shock is thus $0.41/0.19 = 2.13$. The following values are obtained from Eqs. 9 and 5:

Point	Composition [M]	λ	v_c^*
B	$C_L = 0$, $C_N = 0.18$	∞	0.19
C	$C_L = 0$, $C_N = 0.80$	∞	0.41

Since $v^*(C) > v^*(B)$ a simple wave exists between these two states. The concentration profile calculated along the BC path is shown in Fig. 2a. Note that state B is represented by an intermediate plateau followed by a shock where the lysine concentration goes from zero to the feed value. The self-sharpening behavior of the shock is due to the favorable nature of the divalent lysine–ammonium ion exchange. Conversely, the simple wave BC results from the unfavorable exchange of hydrogen ions for ammonium ion. Figure 2a shows the corresponding effluent concentration profiles, which comprise an initial plateau of ammonium ion (C) followed by a simple wave. An intermediate plateau (B) is followed by a shock where the lysine concentration goes from zero to the feed value (A). The agreement with the experimental results is substantial. The main difference is that the concentration profiles between states B and A are more gradual as a result of the slow diffusion of divalent lysine in the resin beads.

Solution for Case 3

In this case monovalent and divalent lysine coexist in the feed. The hodograph plane is shown in Fig. 3b. Point A is the feed and the corresponding resin composition is $q_L = 2.68\,\text{mmol/g}$ and $q_N = 0$. Point C represents the condition $C_L = 0,\ C_N = C^F_{Cl^-}$. The following values are calculated from Eqs. 9 and 5:

Point	Composition [M]	λ	v^*
A	$C_L = 0.20,\ C_N = 0$	-2.19	0.66
C	$C_L = 0,\ C_N = 0.35$	-1.0	0.30

Since $v^*(A) > v^*(C)$ a shock is formed. The shock path is shown by line AB, which intersects the simple wave path starting from point C at point B. Thus, the solution consists of a shock between states A and B, followed by a plateau and a simple wave between states B and C. Point B is found by trial and error from Eq. 10 by setting:

$$\frac{2.68 - q_L(B)}{0.20 - C_L(B)} = \frac{q_N(B)}{C_N(B)}$$

We obtain $C_N = 0.26\,\text{M}$, $C_L = 0.092\,\text{M}$, $q_N = 4.43\,\text{mmol/g}$, $q_L = 0.83\,\text{mmol/g}$, $v^*(B) = 0.24$, and $v_s^*\ (A,B) = 0.14$. The corresponding RV value is $0.41/0.144 = 2.84$. Obviously, the AB shock is due to the favorable nature of

the exchange of divalent lysine for ammonium ion, while the simple wave BC is due to the unfavorable nature of the exchange of monovalent lysine and ammonium ion. Figure 3a shows the calculated effluent concentration profiles. A bipartite behavior can be seen. Initially, following an initial plateau corresponding to state C, there is a single, gradual wave to state B. Then, following an intermediate plateau there is a shock wave of divalent lysine to state A. Again, the local equilibrium model correctly predicts the general shape of the breakthrough curve. Mass transfer effects that are addressed in the next section cause the difference between theory and experimental results. Interestingly, an analogous equilibrium dynamics behavior also has been seen for the anion exchange behavior of chromate ion.[14] In that case, the uptake isotherm is S-shaped. Thus, early breakthrough occurs followed by a shock when the feed concentration is greater than the inflection point of the isotherm.

Lysine Breakthrough and Desorption—Mass Transfer Model

We now consider the general case of a system containing lysine, ammonia, potassium ion, and hydrogen ion. Assuming plug flow and neglecting axial dispersion, the conservation equations are the same as Eqs. 1–4 with the following additional equation and boundary conditions for potassium ion:

$$\rho_b \frac{\partial q_{K^+}}{\partial t} + \varepsilon \frac{\partial C_{K^+}}{\partial t} + u \frac{\partial C_{K^+}}{\partial z} = 0 \tag{11}$$

$$z = 0, C_{K^+} = C^F_{K^+} \tag{12}$$

$$t = 0, C_{K^+} = C^0_{K^+} \tag{13}$$

These equations are now coupled with the following rate equations.

$$\frac{\partial q_L}{\partial t} = -\frac{1}{r^2}\frac{\partial}{\partial r}[r^2(J_{Lys^{++}} + J_{Lys^+})] \tag{14}$$

$$\frac{\partial q_N}{\partial t} = -\frac{1}{r^2}\frac{\partial}{\partial r}[r^2(J_{NH_4^+} + J_{NH_3})] \tag{15}$$

$$\frac{\partial q_{K^+}}{\partial t} = -\frac{1}{r^2}\frac{\partial}{\partial r}[r^2(J_{K^+})] \tag{16}$$

where $J_{Lys^{++}}$ and J_{Lys^+} are the divalent and monovalent lysine fluxes, $J_{NH_4^+}$ and J_{NH_3} are the ammonium ion and free ammonia fluxes, and J_{K^+} is the potassium

ion flux. The following relationships exist between total lysine and total ammonia and the counterion concentrations:

$$q_L = q_{Lys^+} + q_{Lys^{++}} \tag{17}$$

$$q_N = q_{NH_4^+} + q_{NH_3} \tag{18}$$

$$q_0 = q_{H^+} + q_{K^+} + q_{NH_4^+} + q_{Lys^+} + 2q_{Lys^{++}} \tag{19}$$

where q_0 is the total resin ion exchange capacity. Additionally, we have the following two relationships expressing the dissociation equilibrium of divalent lysine and ammonium ion in the resin phase:

$$K_1' = \frac{q_{Lys^+} q_{H^+}}{q_{Lys^{++}}} \tag{20}$$

$$K_N' = \frac{q_{NH_3} q_{H^+}}{q_{NH_4^+}} \tag{21}$$

The first of these two relationships was determined in Part I of this work while the second is discussed later. Combining Eqs. 17–21, we obtain:

$$q_{Lys^{++}} = \frac{(q_0 - q_{K^+} + q_{NH_4^+} - q_{Lys^+}) q_{Lys^+}}{(2q_{Lys^+} + K_1')} \tag{22}$$

$$q_{NH_3} = K_N' \frac{q_{NH_4^+}}{q_0 - q_{K^+} + q_{NH_4^+} - q_{Lys^+} - 2q_{Lys^{++}}} \tag{23}$$

In turn, the derivatives $\partial q_L/\partial t$ and $\partial q_N/\partial t$ can be expressed as:

$$\frac{\partial q_L}{\partial t} = \frac{\partial q_{Lys^+}}{\partial t} + \frac{\partial q_{Lys^{++}}}{\partial q_{Lys^+}} \frac{\partial q_{Lys^+}}{\partial t} + \frac{\partial q_{Lys^{++}}}{\partial q_{NH_4^+}} \frac{\partial q_{NH_4^+}}{\partial t} + \frac{\partial q_{Lys^{++}}}{\partial q_{K^+}} \frac{\partial q_{K^+}}{\partial t} \tag{24}$$

$$\frac{\partial q_N}{\partial t} = \left(1 + \frac{\partial q_{NH_3}}{\partial q_{NH_4^+}}\right) \frac{\partial q_{NH_4^+}}{\partial t} + \frac{\partial q_{NH_3}}{\partial q_{Lys^+}} \frac{\partial q_{Lys^+}}{\partial t} + \frac{\partial q_{NH_3}}{\partial q_{Lys^{++}}} \frac{\partial q_{Lys^{++}}}{\partial t} + \frac{\partial q_{NH_3}}{\partial q_{K^+}} \frac{\partial q_{K^+}}{\partial t} \tag{25}$$

where

$$\frac{\partial q_{Lys^{++}}}{\partial q_{Lys^+}} = \frac{(q_0 - 2q_{Lys^+} - q_{NH_4^+} - q_{K^+}) K_1' - 2q_{Lys^+}^2}{(2q_{Lys^+} + K_1')^2} \tag{26}$$

$$\frac{\partial q_{Lys^{++}}}{\partial q_{NH_4^+}} = \frac{\partial q_{Lys^{++}}}{\partial q_{K^+}} = \frac{-q_{Lys^+}}{(2q_{Lys^+} + K_1')} \tag{27}$$

$$\frac{\partial q_{NH_3}}{\partial q_{NH_4^+}} = K'_N \frac{2q_{Lys^{++}} + q_{Lys^+} + q_{K^+} - q_0}{(q_0 - 2q_{Lys^{++}} - q_{Lys^+} - q_{K^+} - q_{NH_4^+})^2} \tag{28}$$

$$\frac{\partial q_{NH_3}}{\partial q_{K^+}} = K'_1 \frac{q_{NH_4^+} q_{K^+}}{(q_0 - 2q_{Lys^{++}} - q_{Lys^+} - q_{K^+} - q_{NH_4^+})^2} \tag{29}$$

Finally, it is necessary to express the mass transfer fluxes. In Part I of this work,[1] we showed that mass transfer in batch adsorption could be described using the Nernst-Planck model. The corresponding partial differential equation formulation is however computationally cumbersome for column calculations. Thus, as an alternative we use the film model approximation of Carta and Lewus[12] where the mass transfer resistance is represented by steady diffusion through a flat solid film of thickness equal to one fifth of the particle radius. Accordingly, the right hand sides of Eqs. 14–16 are given by:[12]

$$-\frac{1}{r^2}\frac{\partial}{\partial r}[r^2(J_{Lys^{++}} + J_{Lys^+})] = \frac{3m}{r_p^2}\left[2D_{Lys^{++}}\frac{q_{Lys^{++}} - q^*_{Lys^{++}}e^{m/5}}{1 - e^{m/5}} + D_{Lys^+}\frac{q_{Lys^+} - q^*_{Lys^+}e^{m/5}}{1 - e^{m/5}}\right] \tag{30}$$

$$-\frac{1}{r^2}\frac{\partial}{\partial r}[r^2(J_{NH_4^+} + J_{NH_3})] = \frac{3}{r_p^2}\left[D_{NH_4^+}m\frac{q_{NH_4^+} - q^*_{NH_4^+}e^{m/5}}{1 - e^{m/5}} + D_{NH_3}(q^*_{NH_3} - q_{NH_3})\right] \tag{31}$$

$$-\frac{1}{r^2}\frac{\partial}{\partial r}[r^2(J_{K^+})] = \frac{3D_{K^+}}{r_p^2}m\frac{q_{K^+} - q^*_{K^+}e^{m/5}}{1 - e^{m/5}} \tag{32}$$

where m is obtained by solving the equation:

$$\sum_j \left(z_j^2 D_j \frac{q_j - q_j^* \mathrm{e}^{mz_j/5}}{1 - \mathrm{e}^{mz_j/5}}\right) = 0, \quad j = Lys^{++}, Lys^+, NH_4^+, K^+, H^+ \tag{33}$$

The starred quantities appearing in these equations are the interfacial equilibrium resin composition. As shown in Ref.[12] the film model approximation describes the electrostatic coupling of diffusion fluxes while retaining the simplicity and relative accuracy of the classical linear driving force approximation (LDF) for uncoupled diffusion. The equations were solved numerically by discretizing the axial derivatives by backwards finite difference and using subroutine DIVPAG in the IMSL Mathematical and Statistical Libraries (Visual Numerics, Inc., San Ramon, CA) to solve the resulting set of ordinary differential equations as discussed in Ref.[1].

Rate Model Parameters and Results

The equilibrium and rate parameters appearing in the rate model were previously determined in Part I of this work[1] with the exception of the dissociation constant for ammonium ion, K'_N, and the NH_3 diffusivity in the resin phase, which were determined as follows. A packed column was first equilibrated with an ammonia solution and then eluted with distilled, de-ionized water. The results of three such experiments with different initial ammonia concentrations are shown in Fig. 4. At these concentrations, ammonia is primarily in NH_3 form since $pK_N \sim 9.25$.[15] Upon elution with water, the resin remains in the ammonium ion form since the hydrogen ion concentration in water is extremely low. However, any NH_3 initially present in the resin phase is eluted. The elution volume obtained by integrating the elution curves in Fig. 4 is $RV = 0.81 \pm 0.01$. In turn, this is related to the distribution coefficient of NH_3 in the resin by the relationship

$$RV = \varepsilon + (1 - \varepsilon)K_{NH_3}$$

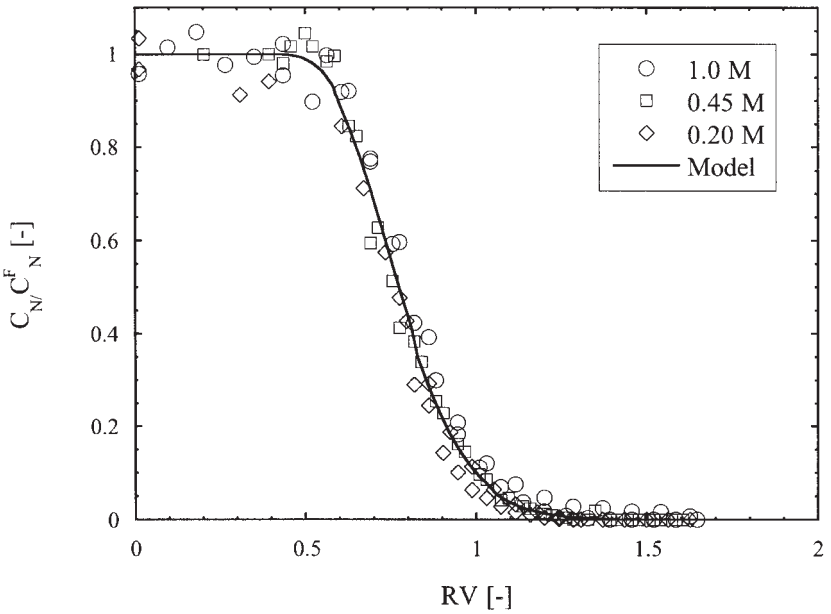

Figure 4. Ammonia elution with distilled, de-ionized water for three different initial ammonia concentrations: $u = 0.0072\,\text{cm/s}$, $L = 10\,\text{cm}$. The line is calculated from a mass transfer model as discussed in the text.

Thus, since $\varepsilon = 0.41$ for this column, $K_{NH_3} = 0.68 \pm 0.01$. For the resin phase we thus have:

$$K'_N = \frac{q_{NH_3} q_{H^+}}{q_{NH_4^+}} = K_{NH_3} \frac{C_{NH_3} q_{H^+}}{q_{NH_4^+}}$$

Two additional relationships can be written. The first is for the dissociation of ammonium ion in solution:

$$K_N = \frac{C_{NH_3} C_{H^+}}{C_{NH_4^+}} = 10^{-9.25}\,\mathrm{M}$$

while the second, determined in Part I of this work,[1] is for the ion exchange equilibrium of the ammonium and hydrogen ions:

$$S_{NH_4^+/H^+} = \frac{q_{NH_4^+} C_{H^+}}{q_{H^+} C_{NH_4^+}} = 1.5$$

Combining the latter three equations yields the final result:

$$K'_N = \frac{K_{NH_3} K_N}{S_{NH_4^+/H^+}} = 2.6 \times 10^{-10}\,\mathrm{M}$$

or $pK'_N \sim 9.6$. This value is somewhat greater than the value in free solution, which can be expected as a result of the high ionic strength in the resin phase (see Ref. 16) and the presence of the charged polymer matrix. Finally, since the resin density is $0.65\,\mathrm{g\,dry/cm^3}$, $K'_N = 4.0 \times 10^{-10}\,\mathrm{mmol/g}$ dry using a dry weight basis.

The last parameter to be determined is the diffusivity of NH_3 in the resin. A value of $D_{NH_3} = 1.9 \times 10^{-6}\,\mathrm{cn^2/s}$ was obtained by fitting the general linear isotherm analytical solution of Carta[17] to the ammonia elution curves as shown in Fig. 4. As expected, this value is lower than in free solution but similar to the diffusivity of ammonium ion. A complete summary of the model parameters is given in Table 1.

Comparisons of experimental breakthrough and desorption curves with model predictions are shown in Figs. 5–7 for lysine feeds at high, low, and intermediate pH. In each case, desorption was with 1 M ammonia. The agreement between experimental and predicted lysine and ammonia concentration profiles is generally very good. The rate model correctly predicts the wave shapes as a function of pH as well as the tailing behavior in the lysine desorption curve. The latter is caused entirely by the slow diffusion of lysine in the resin. Some significant deviations are seen in some cases between experimental and predicted pH profiles. Two factors contribute to

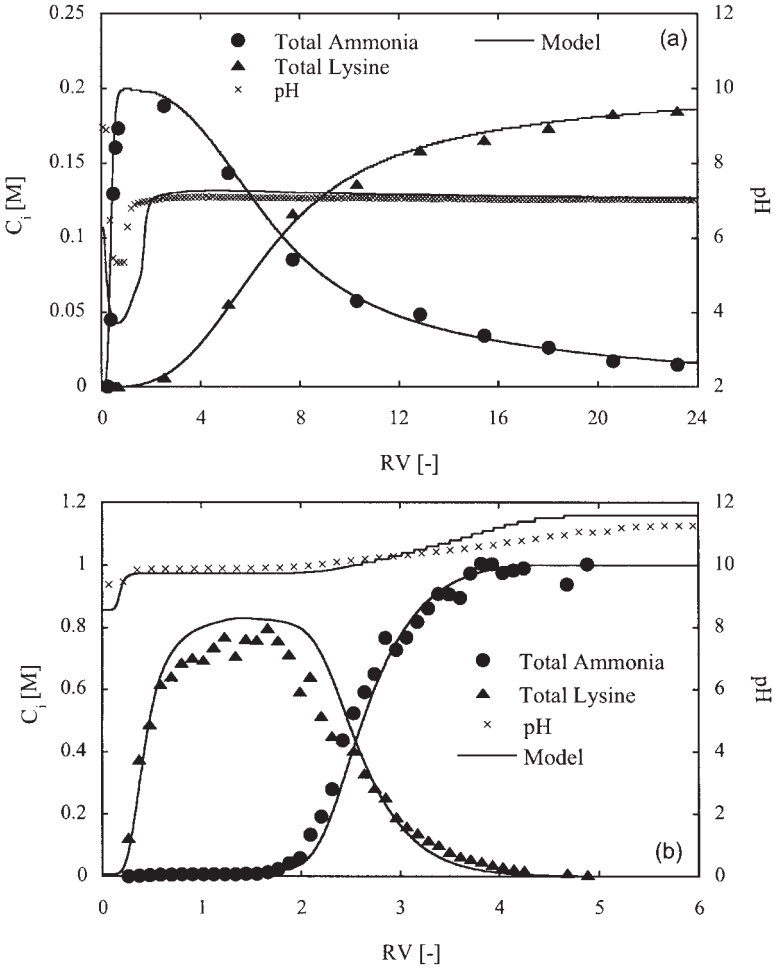

Figure 5. Comparison of experimental and predicted breakthrough and desorption curves. (a) Breakthrough curves for $C_L = 0.20\,\mathrm{M}$, $C_{Cl^-} = 0.20\,\mathrm{M}$, $\mathrm{pH} = 5.57$, (b) desorption with 1 M ammonia: $u = 0.0072\,\mathrm{cm/s}$, $L = 10\,\mathrm{cm}$. Lines are calculated from the mass transfer model.

those differences. The first is that near neutral pH, the pH scale exaggerates differences in hydrogen ion concentration. For example a difference between pH 4 and pH 5 translates to a hydrogen ion concentration difference around $10^{-4}\,\mathrm{M}$. This is much smaller than all other ion concentrations are so that it cannot be predicted exactly. Another reason is that the solution

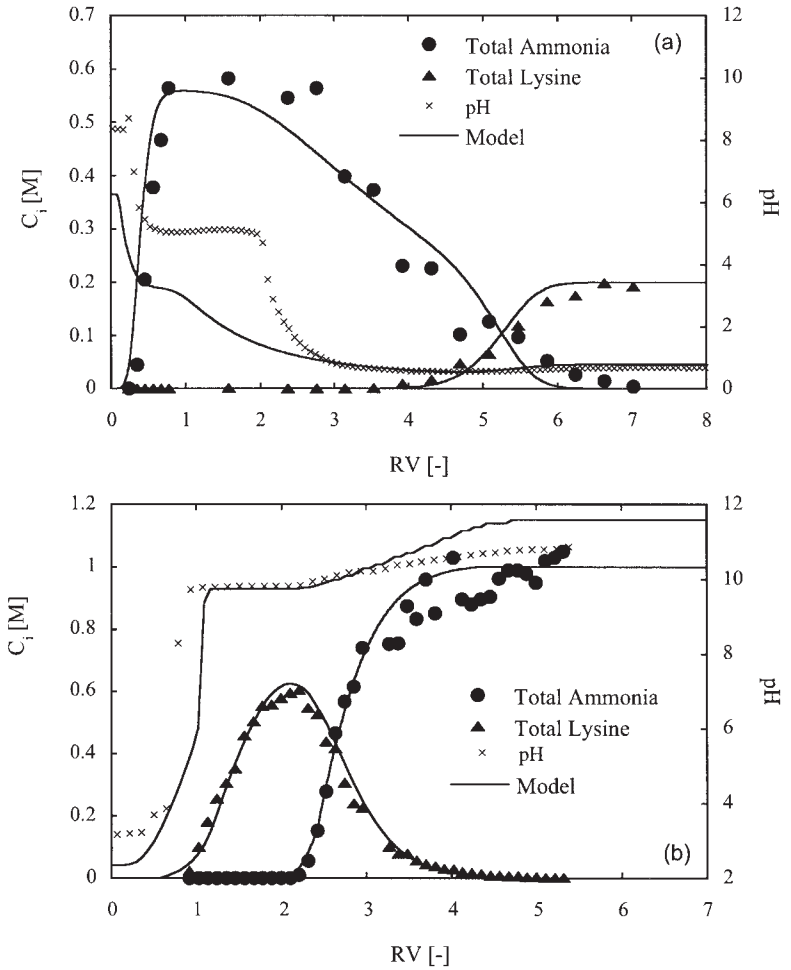

Figure 6. Comparison of experimental and predicted breakthrough and desorption curves. (a) Breakthrough curves for $C_L = 0.20\,\text{M}$, $C_{Cl^-} = 0.56\,\text{M}$, pH = 0.80, (b) desorption with 1 M ammonia: $u = 0.0072\,\text{cm/s}$, $L = 10\,\text{cm}$. Lines are calculated from the mass transfer model.

phase is treated as ideal in the model; i.e., activity coefficients were assumed to be unity. The pH meter, however, measures the activity of hydrogen ion, which is likely to have an effect especially at very high concentrations.

The effect of flow rate is shown in Figs. 8 and 9 for lysine breakthrough at high and low pH and desorption with 1 M ammonia. Spreading of the

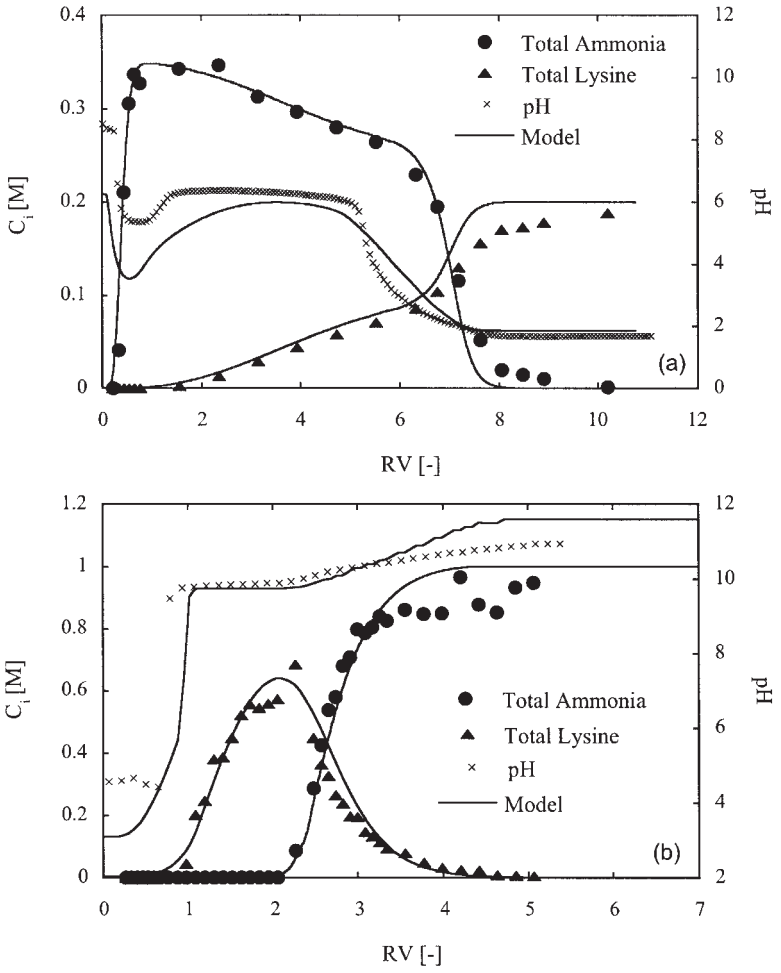

Figure 7. Comparison of experimental and predicted breakthrough and desorption curves. (a) Breakthrough curves for $C_L = 0.20\,\text{M}$, $C_{Cl^-} = 0.35\,\text{M}$, pH = 1.85, (b) desorption with 1 M ammonia: $u = 0.0072\,\text{cm/s}$, $L = 10\,\text{cm}$. Lines are calculated from the mass transfer model.

concentration profiles is increased substantially as a result of the reduced residence time. In particular, tailing of the desorption curve occurs to a greater extent in excellent agreement with model predictions.

The effect of potassium ion present in the lysine feed as an impurity is shown in Figs. 10 and 11. For the high pH feed (Fig. 10), breakthrough

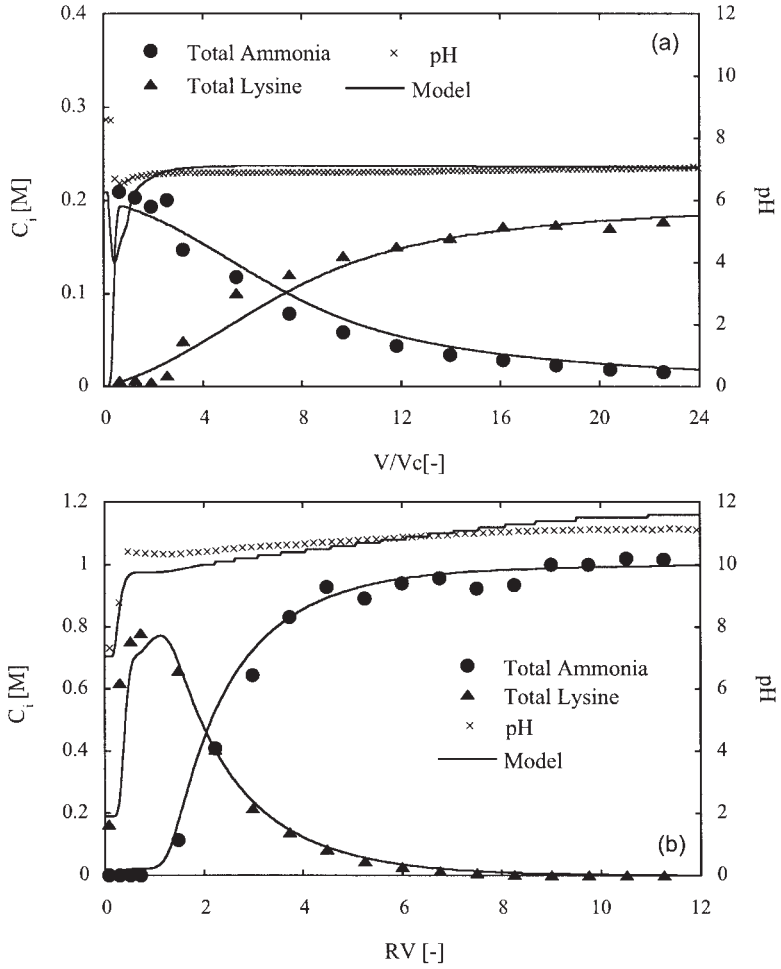

Figure 8. Comparison of experimental and predicted breakthrough and desorption curves at high flow rate. (a) Breakthrough curves for $C_L = 0.20\,\text{M}$, $C_{Cl^-} = 0.20\,\text{M}$, pH = 5.57, (b) desorption with 1 M ammonia: $u = 0.074\,\text{cm/s}$, $L = 20\,\text{cm}$. Lines are calculated from the mass transfer model.

of potassium ion occurs after breakthrough of lysine as potassium is more favorably bound by the resin. Thus, upon desorption with ammonia, a significant potassium peak contaminates the lysine recovered (Fig. 10b). Conversely, for the low pH feed, potassium ion breaks through ahead of the lysine front and negligible contamination of the lysine desorption peak is seen in

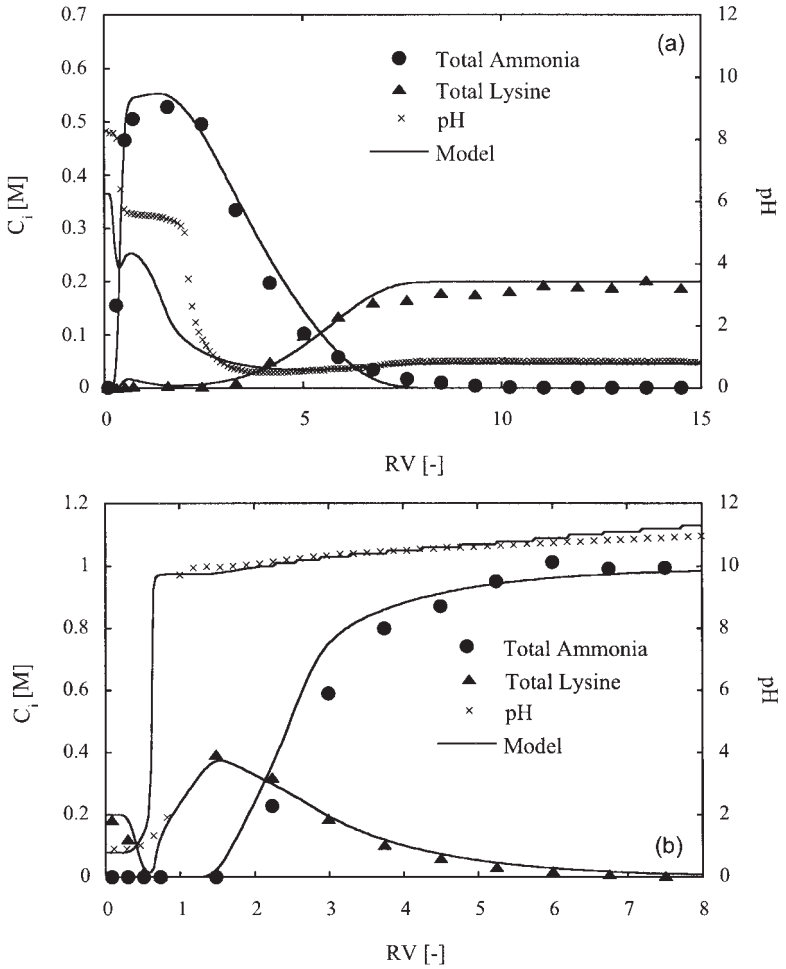

Figure 9. Comparison of experimental and predicted breakthrough and desorption curves at high flow rate. (a) Breakthrough curves for $C_L = 0.20\,\text{M}$, $C_{Cl^-} = 0.56\,\text{M}$, pH = 0.80, (b) desorption with 1 M ammonia: $u = 0.074\,\text{cm/s}$, $L = 20\,\text{cm}$. Lines are calculated from the mass transfer model.

Fig. 11b. This occurs as a result of the favorable exchange of divalent lysine. The model predictions are once again in good agreement with the experimental results.

A final consideration is the ability of the rate model to predict the reversible interconversion of monovalent and divalent lysine in the column.

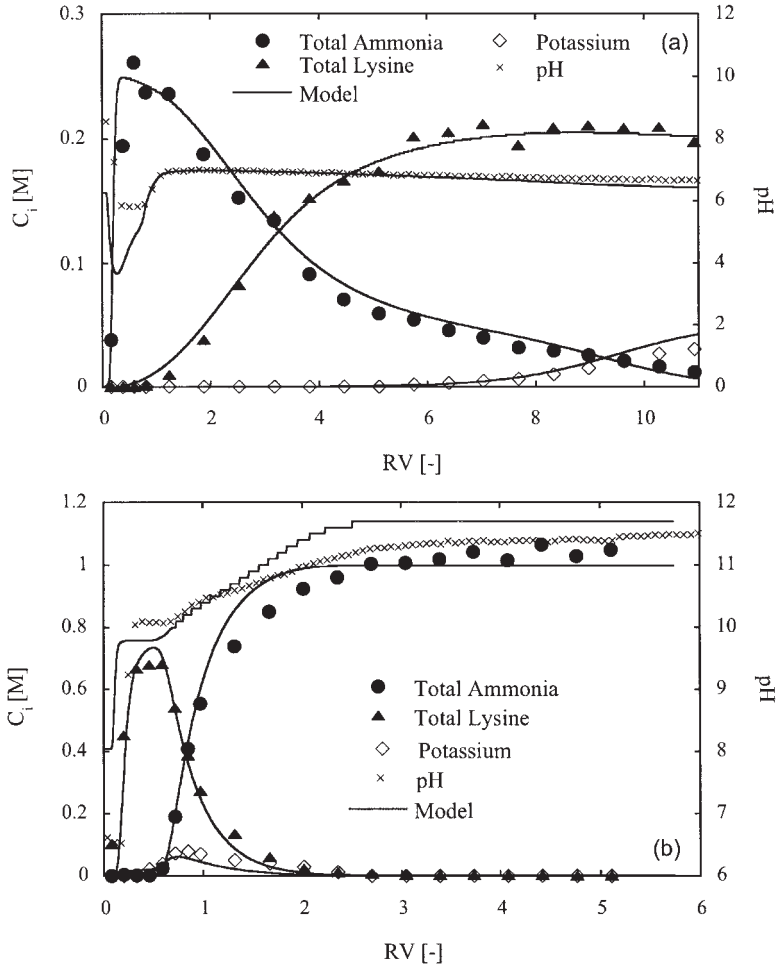

Figure 10. Comparison of experimental and predicted breakthrough and desorption curves with potassium in lysine feed. (a) Breakthrough curves for $C_L = 0.20\,\text{M}$, $C_{K^+} = 0.05\,\text{M}$, $C_{Cl^-} = 0.25\,\text{M}$, (b) desorption with 1 M ammonia: $u = 0.0072\,\text{cm/s}$, $L = 10\,\text{cm}$. Lines are calculated from the mass transfer model.

To test this effect, a column was initially equilibrated with a divalent lysine solution with $C_L = 0.20\,\text{M}$ and $C_{Cl^-} = 0.56\,\text{M}$ and then supplied with a monovalent lysine feed with $C_L = 0.20\,\text{M}$ and $C_{Cl^-} = 0.20\,\text{M}$. The results are shown in Fig. 12. It can be seen that as the chloride ion concentration is changed from 0.56 to 0.20 M, the effluent lysine concentration

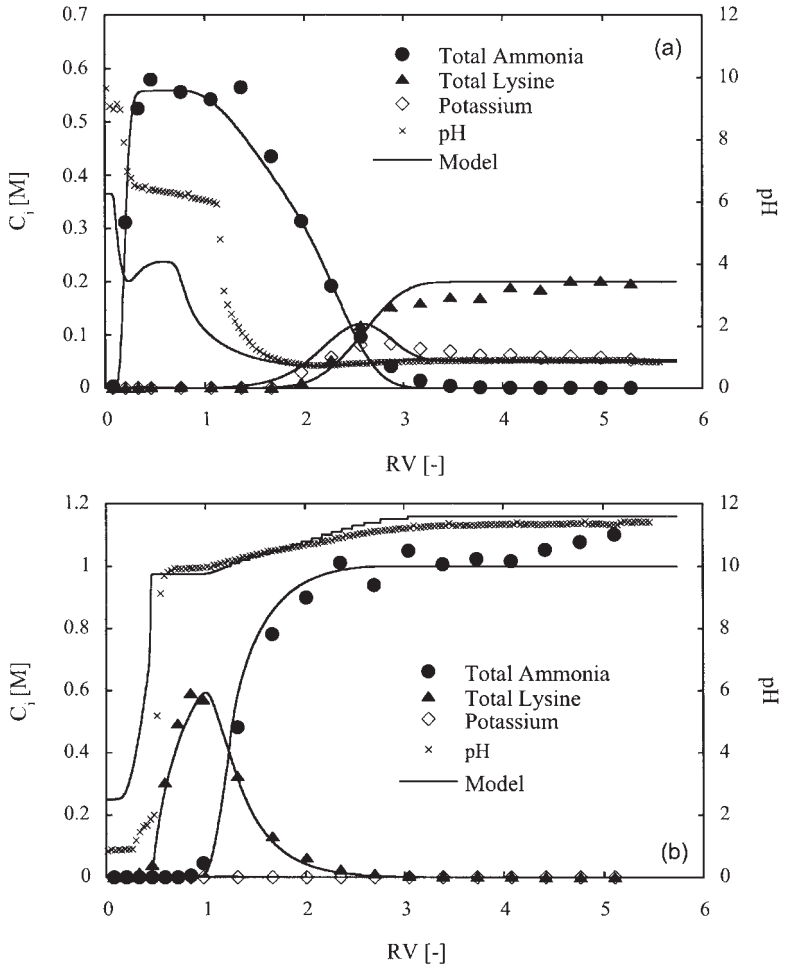

Figure 11. Comparison of experimental and predicted breakthrough and desorption curves with potassium in lysine feed. (a) Breakthrough curves for $C_L = 0.20\,\text{M}$, $C_{K^+} = 0.05\,\text{M}$, $C_{Cl^-} = 0.61\,\text{M}$, (b) desorption with 1 M ammonia: $u = 0.0072\,\text{cm/s}$, $L = 10\,\text{cm}$. Lines are calculated from the mass transfer model.

temporarily decreases. This occurs because divalent lysine in the resin is converted to the monovalent form allowing the uptake of additional lysine. After achieving equilibrium, the feed was switched again to the divalent lysine solution with $C_L = 0.20\,\text{M}$ and $C_{Cl^-} = 0.56\,\text{M}$. In this case, as seen in Fig. 12, the effluent lysine concentration shows a fairly sharp peak

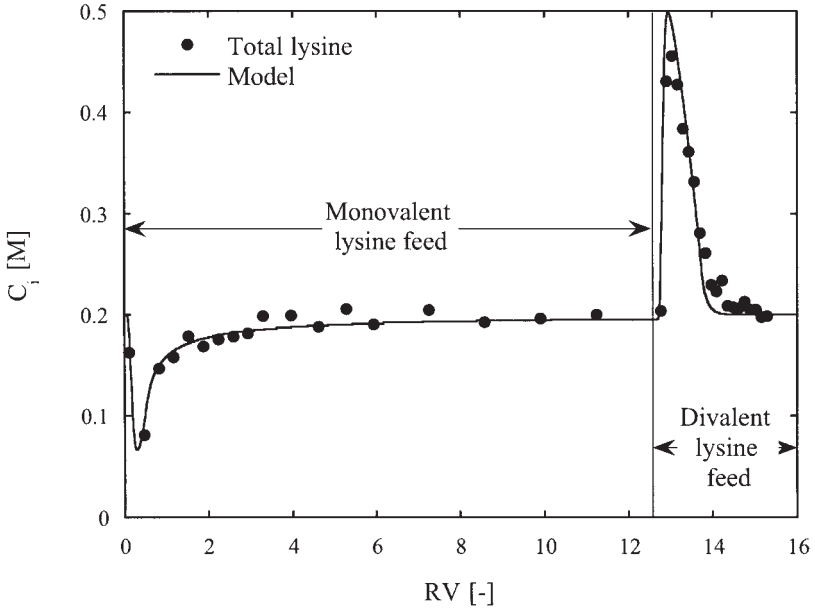

Figure 12. Comparison of experimental and predicted lysine effluent concentration. The column was initially equilibrated with divalent lysine. Initial monovalent lysine feed: $C_L = 0.20\,\text{M}$, $C_{Cl^-} = 0.20\,\text{M}$; divalent lysine feed: $C_L = 0.20\,\text{M}$, $C_{Cl^-} = 0.56\,\text{M}$; $u = 0.015\,\text{cm/s}$; $L = 20\,\text{cm}$. Lines are calculated from the mass transfer model.

approaching 0.5 M. This occurs as monovalent lysine in the resin is converted to the divalent form causing lysine to be desorbed from the resin in order to accommodate the increased charge. As seen in Fig. 12, the rate model predictions are in excellent agreement with the observed concentration profiles.

CONCLUSIONS

Two modeling approaches were adopted to describe the column adsorption and desorption behavior of lysine cation exchange. The first approach, based on the assumption of local equilibrium, predicts the effects of lysine feed pH on the breakthrough curve. A gradual wave is obtained when the feed contains predominately monovalent lysine, while a shock is obtained when the divalent form is dominant. At intermediate lysine feed

pH, a complex breakthrough curve comprising a gradual wave followed by a shock is obtained. The second modeling approach is based on a rate model incorporating equilibrium and diffusion parameters determined in Part I of this work. The model employs a film model approximation to describe interphase mass transfer and is found to provide a quantitative prediction of the lysine breakthrough curves. The model also predicts the lysine desorption behavior, the effects of potassium present as an impurity in the lysine feed, and the reversible interconversion of monovalent and divalent lysine in the column.

As seen experimentally as well as through the model predictions in Figs. 5 and 6, the feed pH has an interesting effect on the lysine dynamic binding capacity. Although the equilibrium uptake capacity at high pH (Fig. 5) is nearly double the capacity observed at low pH (Fig. 6), lysine breakthrough actually occurs earlier in Fig. 5 than it does in Fig. 6. This occurs because while the capacity is greater, the exchange equilibrium is unfavorable for monovalent lysine, which is predominant in Fig. 5. Although diffusion of divalent lysine in the resin is slow, the favorable nature of the ion exchange equilibrium still results in a sharper breakthrough curve. While it is not easy to predict a priori which of these effects is dominant for different conditions, it appears that optimum conditions can be chosen following the modeling approaches developed in this work.

NOMENCLATURE

C_i	concentration of species i in solution (mol/L)
C_0	total co-ion concentration (mol/L)
K_1, K_2, K_3	lysine dissociation constants (mol/L)
K_1'	resin phase dissociation constant for divalent lysine (mol/L)
K_N	ammonia dissociation constant (mol/L)
K_N'	resin phase ammonia dissociation constant (mol/L)
K_{NH_3}	partition coefficient for NH_3 in the resin
D_i	resin phase diffusivity of species i (cm^2/s)
L	column length (cm)
q_i	concentration of species i in resin phase (mmol/g)
q_0	resin ion exchange capacity (mequiv/g)
r	particle radial coordinate (cm)
r_p	particle radius (cm)
$S_{i/j}$	selectivity coefficient of the exchange of ion i and j
t	time (s)
u	superficial velocity (cm/s)
v	interstitial velocity (cm/s)

v_c	characteristic velocity for simple waves (cm/s)
v_s	characteristic velocity for shock waves (cm/s)
z	column axial coordinate (cm)
z_i	ion charge
ε	column void fraction
λ	characteristic slope
ρ_b	packed bed resin density (g/cm^3)

ACKNOWLEDGMENT

This research was supported by Ajinomoto Co., Inc.

REFERENCES

1. Nagai, H.; Carta, G. Lysine adsorption on cation exchange resin-I. Ion exchange equilibrium and kinetics. Sep. Sci. Technol. **2004**, *39*, 3691–3710.
2. Kawakita, T.; Ito, Y.; Sano, C.; Ogura, T.; Saeki, M. Breakthrough curve of lysine on a column of a strong cation exchange resin of the ammonium form. Sep. Sci. Technol. **1991**, *26*, 619–635.
3. Van Walsem, H.J.; Thompson, M.C. Simulated moving bed in the production of lysine. J. Biotechnol. **1997**, *59*, 127–132.
4. Ruthven, D.M. *Principles of Adsorption and Adsorption Processes*; Wiley: New York, 1984.
5. LeVan, M.D.; Carta, G.; Yon, C. *Adsorption and ion exchange. Section 16 in Perry's Chemical Engineers' Handbook*, 7th Ed.; Green, D.W., Ed.; McGraw-Hill: New York, 1997.
6. Carta, G.; Saunders, M.S.; DeCarli, J.P. II; Vierow, J.B. Dynamics of fixed-bed separations of amino acids by ion exchange. AIChE Symp. Ser. **1988**, *84*, 54–61.
7. Saunders, M.S.; Vierow, J.B.; Carta, G. Uptake of phenylalanine and tyrosine by a strong acid cation exchanger. AIChE J. **1989**, *35*, 53–68.
8. DeCarli, J.P., II; Carta, G.; Byers, C.H. Displacement separations by continuous annular chromatography. AIChE J. **1990**, *36*, 1220–1228.
9. Carta, G.; Dinerman, A.A. Displacement chromatography of amino acids: Effects of selectivity reversal. AIChE J. **1994**, *40*, 1618–1628.
10. Carta, G.; Saunders, M.S.; Mawenkang, F. Studies on the diffusion of amino acids in ion exchange resins. In *Fundamentals of Adsorption*; Mersmann, A.B., Scholl, S.E., Eds.; United Engineering Trustees: New York, 1991; 181–190.

11. Melis, S.; Markos, J.; Cao, G.; Morbidelli, M. Separation between amino acids and inorganic ions through ion exchange: Development of a lumped model. Ind. Eng. Chem. Research **1996**, *35*, 3629–3636.
12. Carta, G.; Lewus, R.K. Film model approximation for particle-diffusion-controlled multicomponent ion exchange. Sep. Sci. Technol. **1999**, *34*, 2685–2697.
13. Helfferich, F.; Klein, G. *Multicomponent Chromatography: Theory of Interference*; Marcel-Dekker: Ann Arbor, MI, 1970.
14. Sengupta, A.K.; Lim, L. Modeling chromate ion-exchnage processes. AIChE J. **1988**, *34*, 2019–2029.
15. Weast, R.C. *CRC Handbook of Chemistry and Physics*, 59th Ed.; CRC Press: Boca Raton, FL, 1978.
16. Maeda, M.; Kato, K. Dissociation constants of ammonium ion and activity coefficients of ammonia in ammonium nitrate solutions. J. Chem. Eng. Data **1995**, *40*, 253–256.
17. Carta, G. Exact analytic solution of a mathematical model for chromatographic operations. Chem. Eng. Sci. **1988**, *43*, 2877–2883.

Received March 2, 2004
Accepted September 14, 2004